Supporting Information

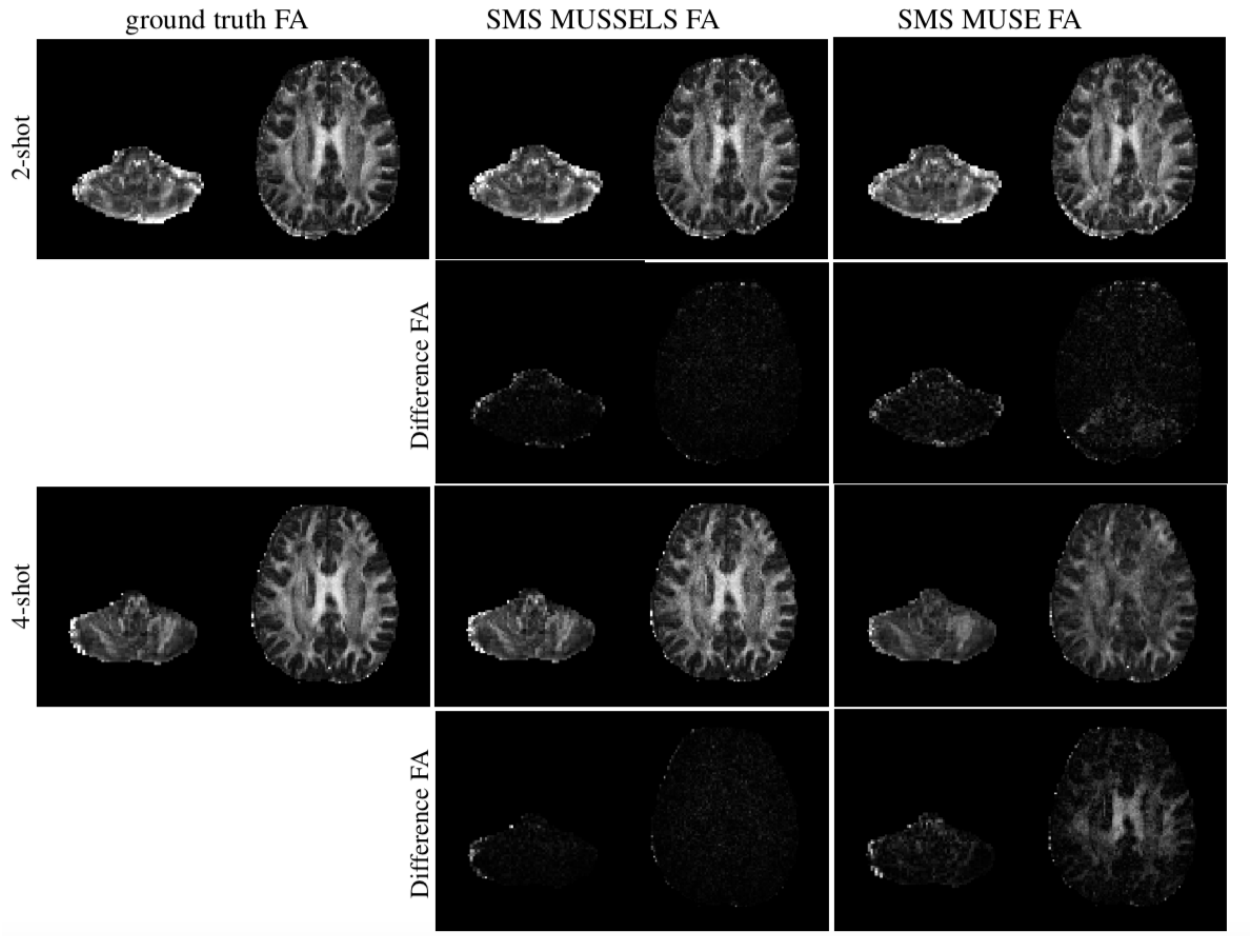

Figure S1: The quantitative analysis of the reconstruction as a function of multi-shot factor for MB=2. The first and the third row display the FA maps from the 2-shot and the 4-shot data respectively. The second and the fourth row displays the difference FA maps for each reconstruction compared to the ground truth reconstruction. The results from both SMS MUSSELS (middle column) and SMS MUSE (right column) are included.All maps are displayed on a color scale of [0 1].

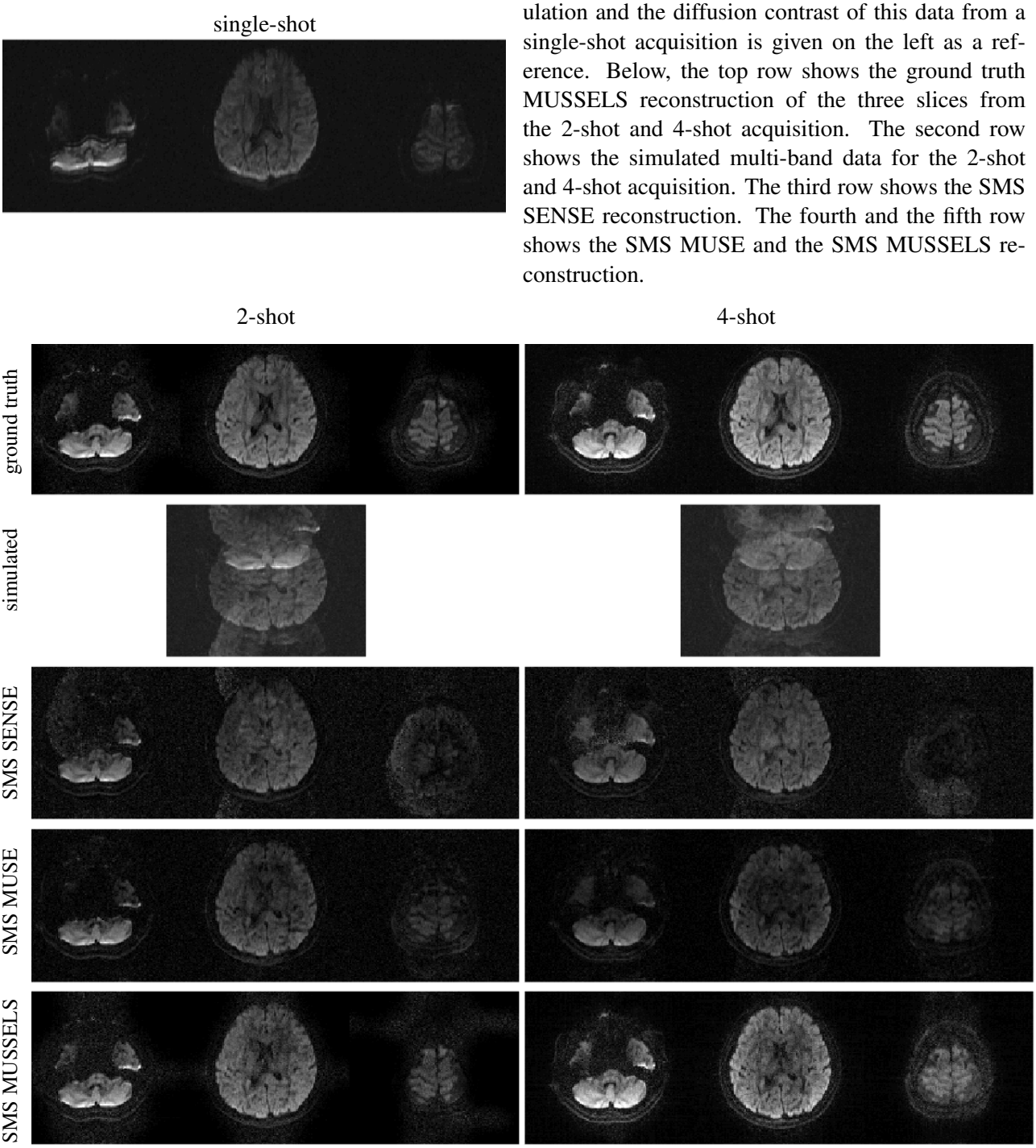

Figure S2: Simulation study for MB=3 using 2-shot and 4-shot data. The slice locations used for the simulation and the diffusion contrast of this data from a single-shot acquisition is given on the left as a reference. Below, the top row shows the ground truth MUSSELS reconstruction of the three slices from the 2-shot and 4-shot acquisition. The second row shows the simulated multi-band data for the 2-shot and 4-shot acquisition. The third row shows the SMS SENSE reconstruction. The fourth and the fifth row shows the SMS MUSE and the SMS MUSSELS reconstruction.

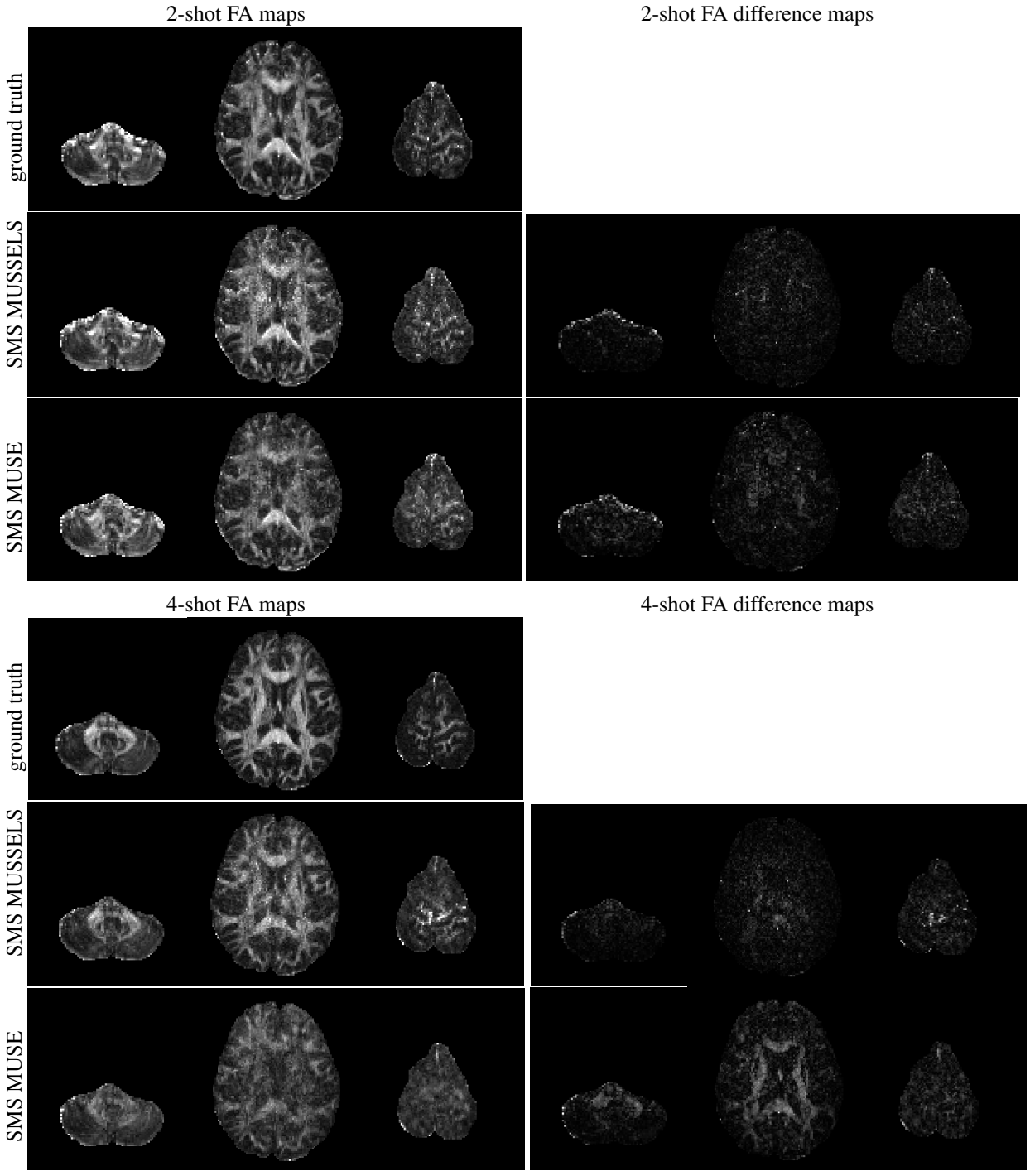

Figure S3: Change in FA maps as a function of multi-shot factor for MB=3. The FA maps computed from the SMS MUSSELS and the SMS MUSE are also compared.

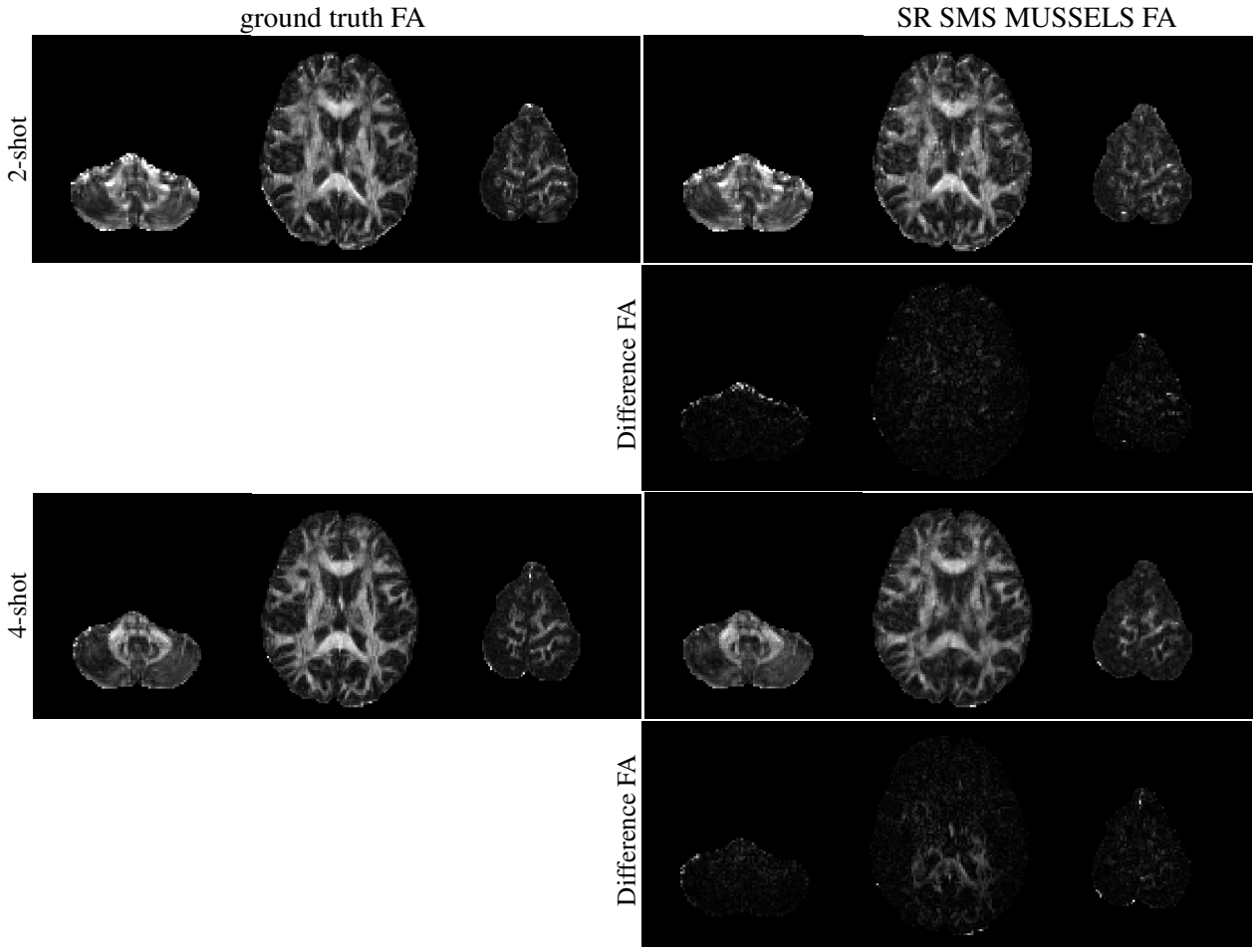

Figure S4: The FA maps and the difference FA maps computed for SR SMS MUSSELS at MB=3.

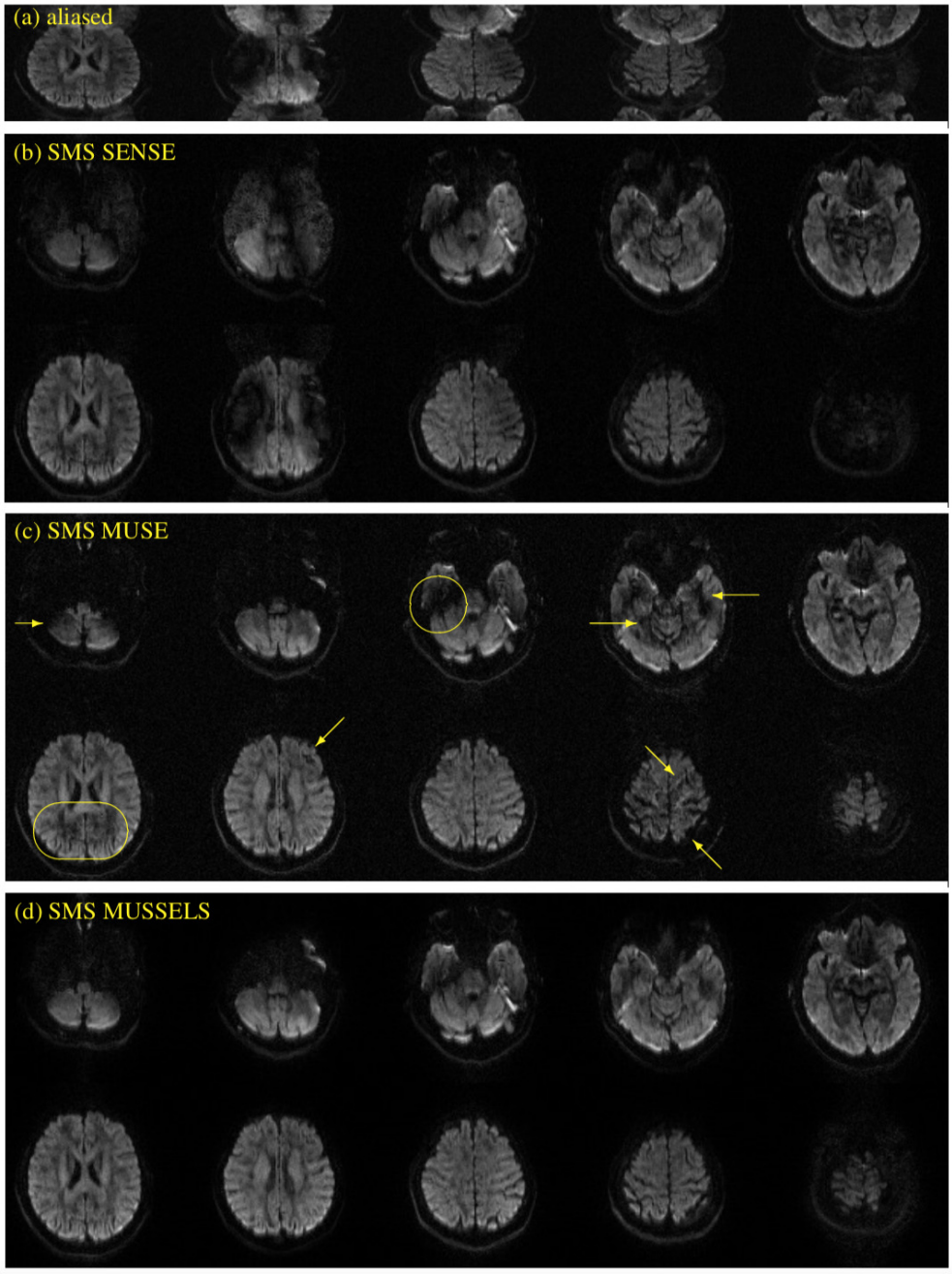

Figure S5: In-vivo multi-band multi-shot data for MB=2 and Ns=2. (a) shows the images from different slice location from the multi-band acquisition before slice unfolding. (b) shows a SMS SENSE reconstruction, (c) shows the SMS MUSE reconstruction and (d) shows the SMS MUSSELS reconstruction.

Figure S6: In-vivo multi-band multi-shot data for MB=3 and Ns=2. (a) shows the images from different slice location from the multi-band acquisition before slice unfolding. (b) shows a SMS SENSE reconstruction, (c) shows the SMS MUSE reconstruction, (d) shows the SMS MUSSELS reconstruction and (e) shows the SR SMS MUSSELS reconstruction.

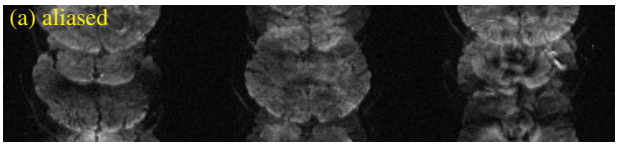

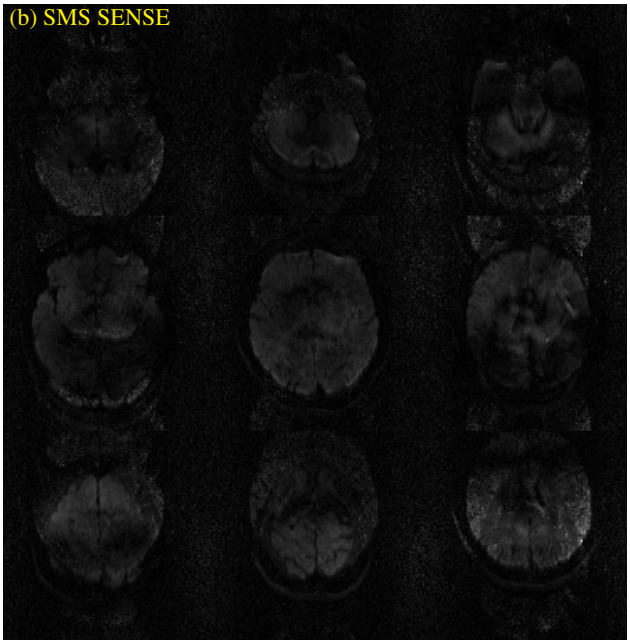

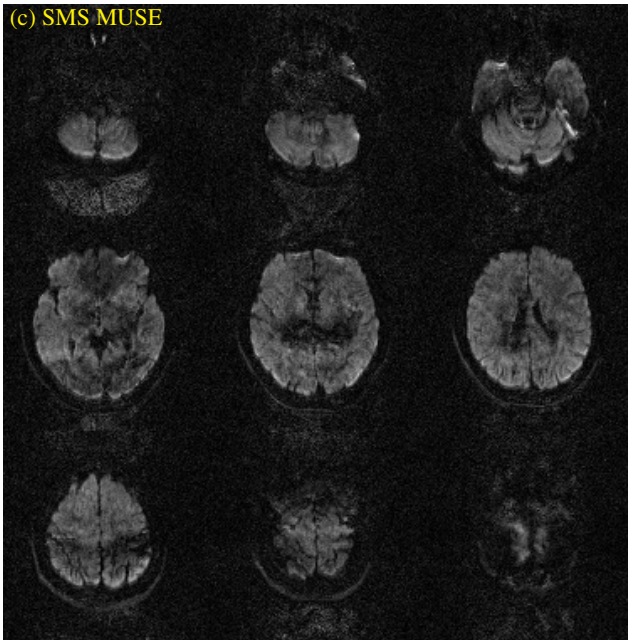

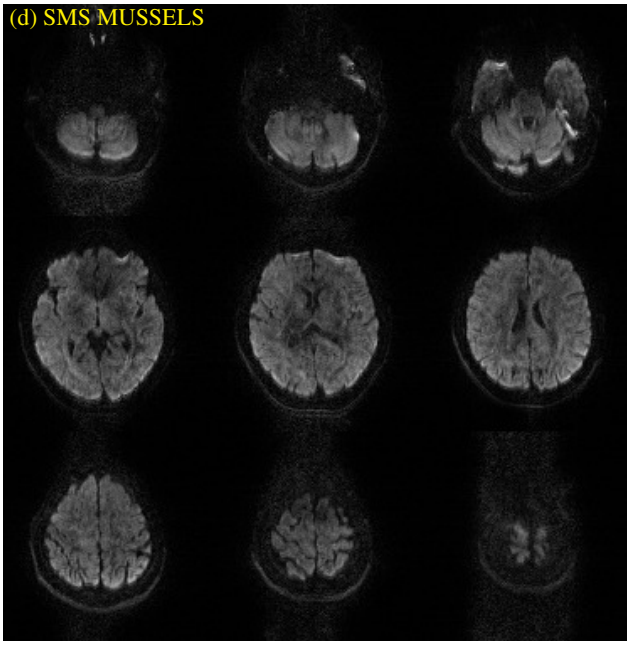

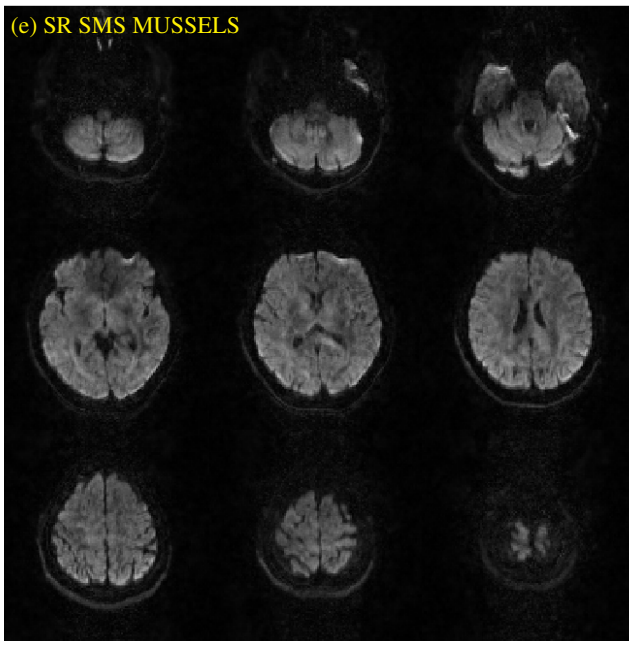

Figure S7: In-vivo multi-band multi-shot data for MB=3 and Ns=4. (a) shows the images from different slice location from the multi-band acquisition before slice unfolding. (b) shows a SMS SENSE reconstruction, (c) shows the SMS MUSE reconstruction, (d) shows the SMS MUSSELS reconstruction and (e) shows the SR SMS MUSSELS reconstruction.

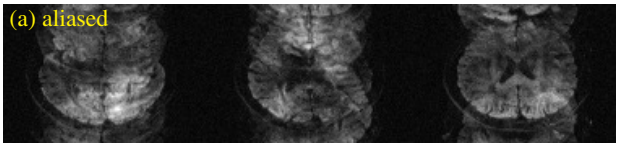

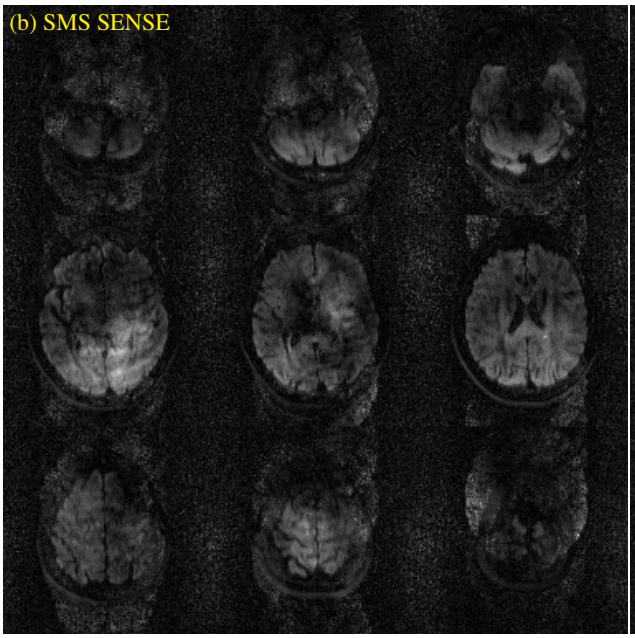

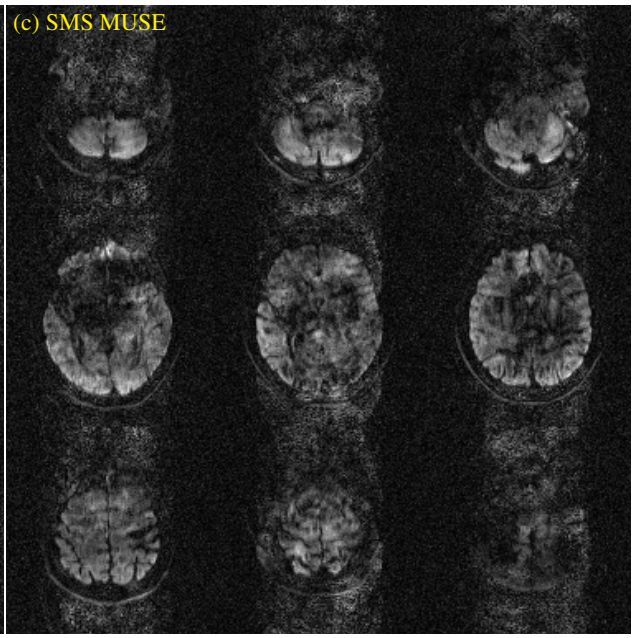

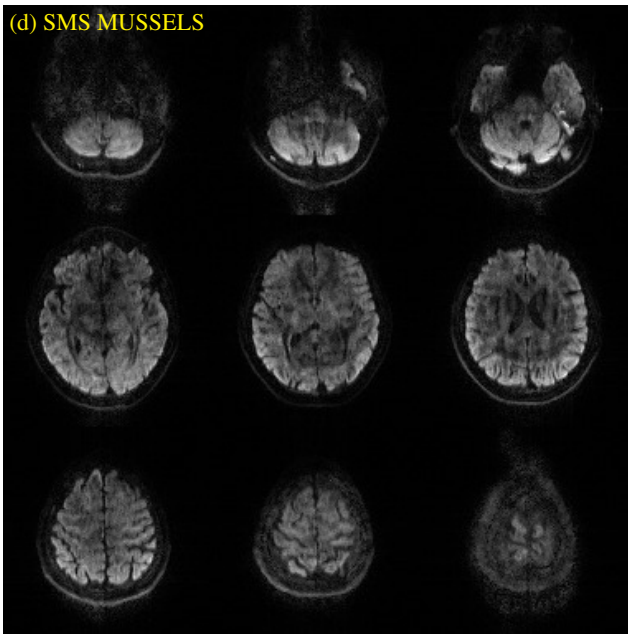

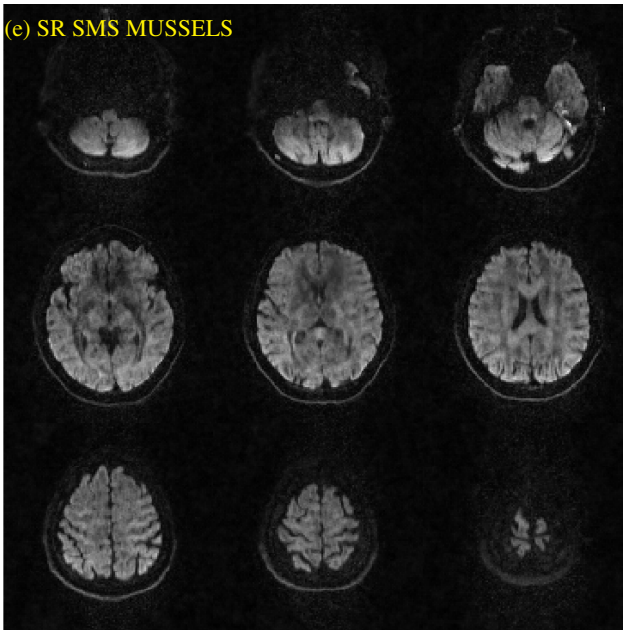

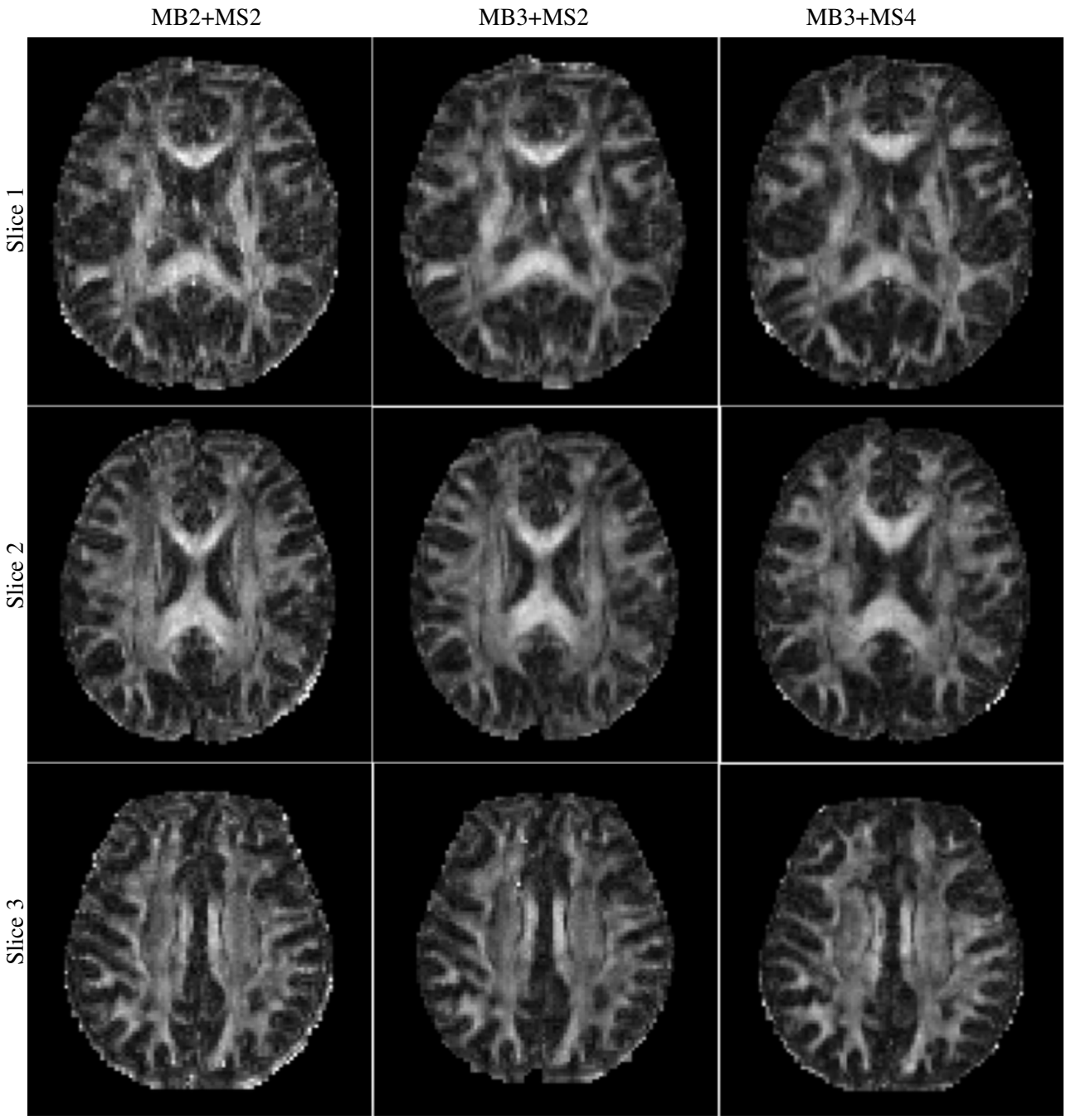

Figure S8: The FA maps from a few typical slices computed for various multi-band and multi-shot factors.

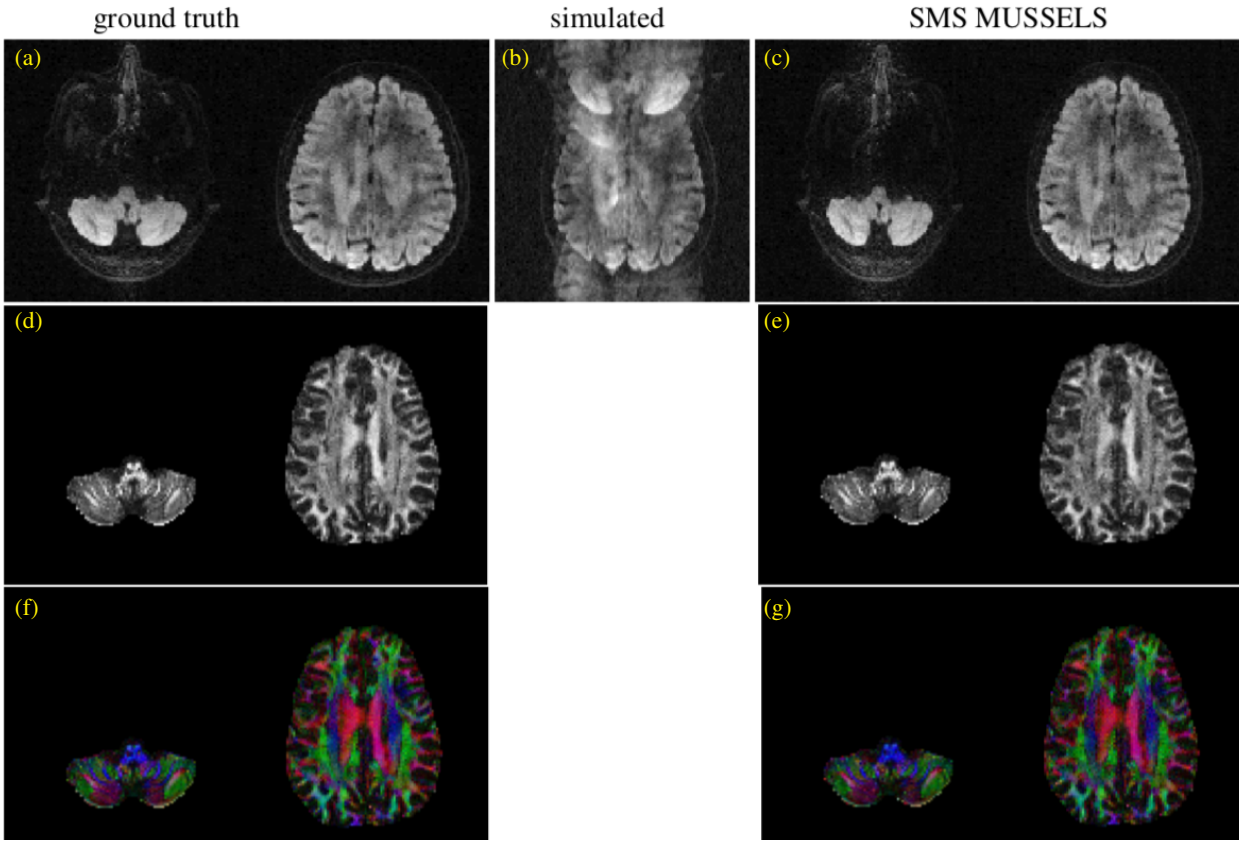

Figure S9: Simulation study of 8-shot data for MB=2. (a) the ground truth MUSSELS reconstructed images for the 8-shot data from the two slices that were used for the multi-band simulation. (b) shows the resulting image from the simulated multi-band data, (c) shows the SMS MUSSELS reconstruction that unfolded the DWIs without phase artifacts. (d) and (f) show the FA and the direction encoded FA maps from the ground truth reconstruction of 25 DWIs. (e) and (g) show the corresponding maps from the SMS MUSSELS reconstruction.

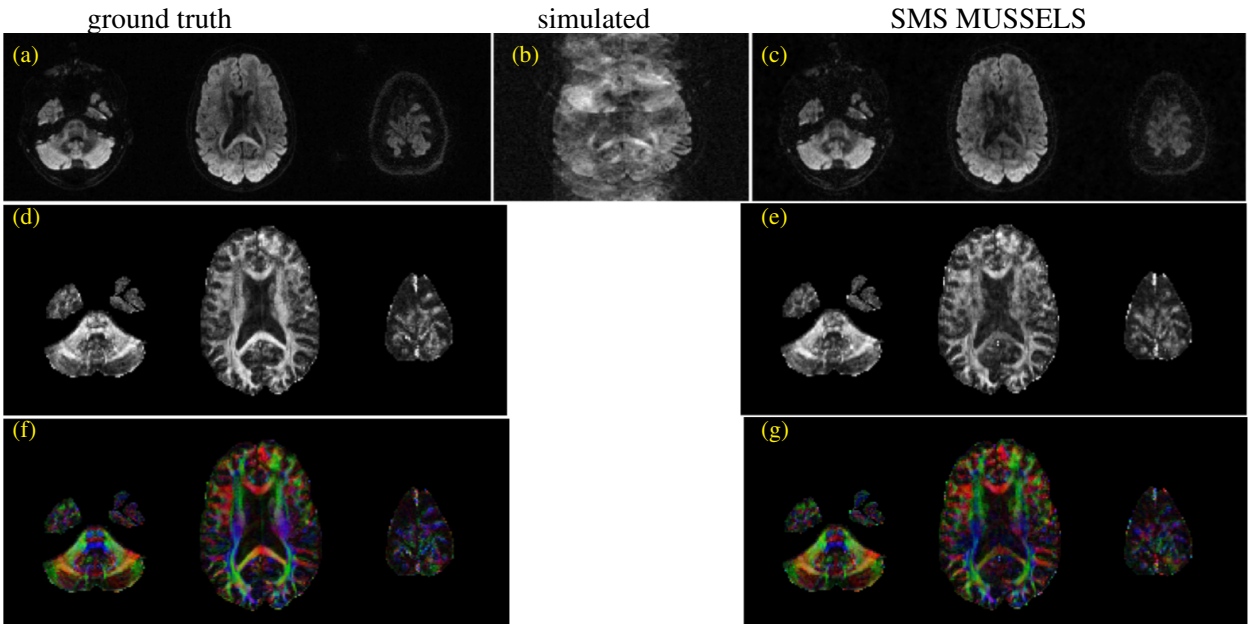

Figure S10: Simulation study of 8-shot data for MB=3. (a) the ground truth SR MUSSELS reconstructed images for the 8-shot data from the two slices that were used for the multi-band simulation. (b) shows the resulting image from the simulated multi-band data, (c) shows the SR SMS MUSSELS reconstruction that unfolded the DWIs without phase artifacts. (d) and (f) show the FA and the direction encoded FA maps from the ground truth reconstruction of 25 DWIs. (e) and (g) show the corresponding maps from the SR SMS MUSSELS reconstruction.

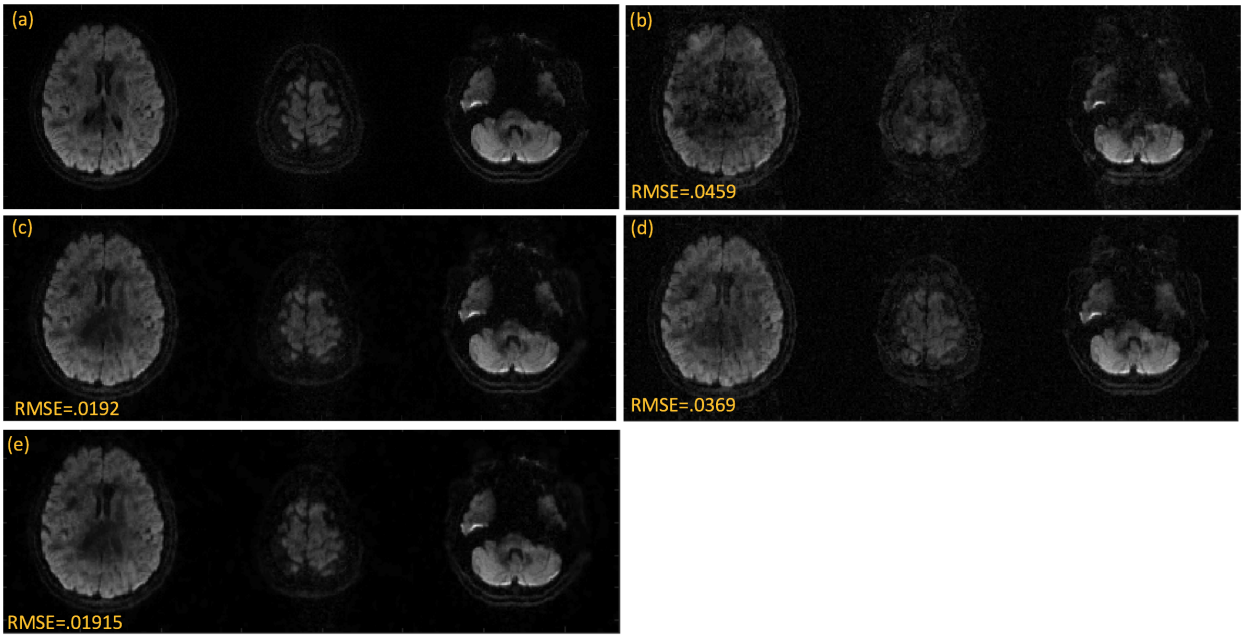

Figure S11: (a) the ground truth reconstruction for a given DWI for MB=3 and N_s=4, (b) SMS MUSE reconstruction employing phase estimate from a regularized SENSE reconstruction, (c) SR SMS MUSSELS reconstruction, (d) SMS MUSE reconstruction employing phase estimates from the SR SMS MUSSELS reconstruction. The better phase estimate from the SR SMS MUSSELS reconstruction improved the SMS MUSE reconstruction. (e) a modified SMS MUSE + SR MUSSELS reconstruction explicitly using phase estimates in the encoding function and employing a low-rank regularization. This reconstruction converged to the SR SMS MUSSELS reconstruction in (c) as expected.

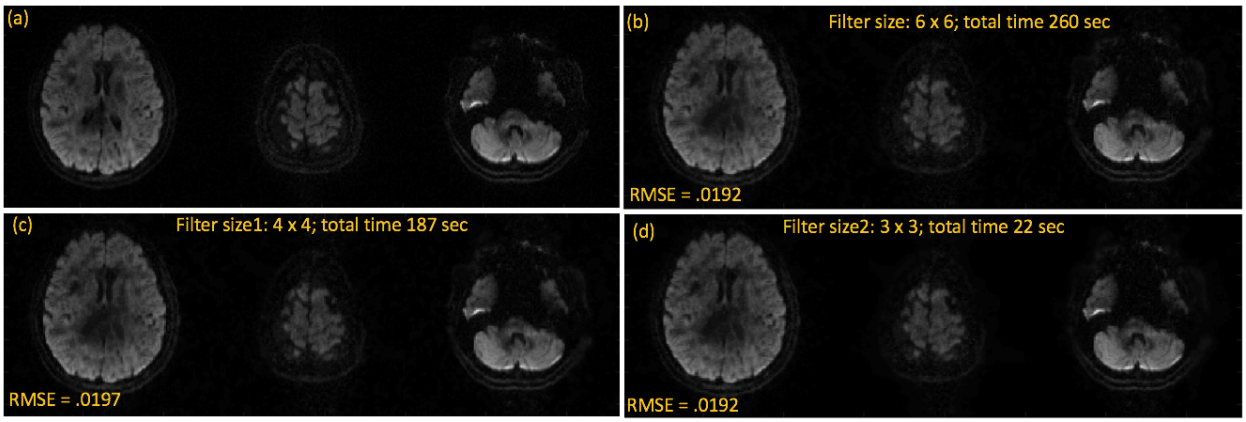

Figure S12: The purpose of this experiment is to show that an iterative SMS MUSSELS scheme can be designed to iteratively remove phase errors employing several small band-pass filters. (a) the ground truth reconstruction, (b) SR SMS MUSSELS reconstruction using 6 x 6 filter that resulted in the minimum RMSE for this DWI, (c) SR SMS MUSSELS reconstruction using 4 $\times$ 4 filter, which gives a higher RMSE if used by itself; (d) reconstruction from the second round of SR SMS MUSSELS using 3 $\times$ 3 filter. In the second round of the iterative SR SMS MUSSELS reconstruction, the phase estimate from (c) was absorbed into the encoding function similar to the SMS MUSE reconstruction. The second iteration also used the magnitude image of (c) as the initial estimate. The second round thus removed any residual phase aliasing and matched the RMSE of filter size 6 $\times$ 6. This approach provide a slight advantage in the computation time. Whereas (b) took 260 sec, running (c) & (d) back to back took 209 sec.

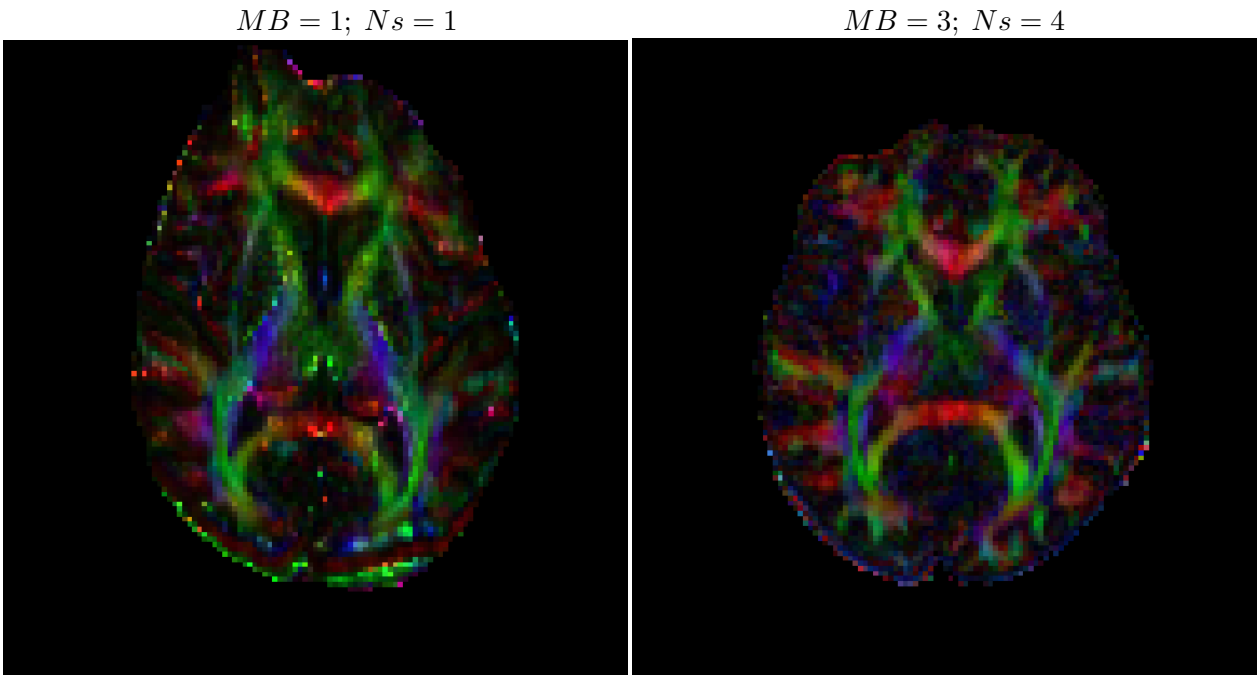

Figure S13: The direction color encoded FA maps from (a) single-band single-shot data and (b) multi-band multi-shot data. The geometric distortions effects and the image quality show significant improvement for the latter case.